INVESTIGATING ICEQUAKES ON ENCELADUS USING AN ANTARCTIC ANALOG: APPLICATION OF SEISMIC AND MACHINE-LEARNING TECHNIQUES TO CHARACTERIZE TIDALLY INDUCED SEISMICITY ALONG ICY RIFTS. K. G. Olsen[1,2], N. C. Schmerr[3], MH Huang[3], T. A. Hurford[2], K. M. Brunt[2,3], [1]USRA, Columbia, MD, [2]NASA Goddard Space Flight Center, Greenbelt, MD (kira.olsen@nasa.gov), [3]University of Maryland, College Park, MD.

Introduction: The icy shell of Enceladus is riven with fractures, including the four large Tiger Stripe fractures which lie at the moon's south pole (Figure 1c). Jets of water vapor and ice particles emanating from the Tiger stripes [1] provide strong evidence that these fractures connect to subsurface reservoirs of liquid water, making them a key target for study of ice-shell structure, habitability, and more. The Tiger Stripe fractures exhibit offset features along their ~100 km lengths which show that significant slip has occurred in these locations, driven by continuous cycles of tidal stresses [2]. Like faults on Earth's surface, the Tiger Stripe Fractures are likely caused by, and the cause of, ongoing seismic activity. Observation and analysis of Enceladean seismicity by a future landed mission will present a valuable opportunity to study energy release within an icy shell and to advance understanding of icy-crust deformation as well as interrogate interior structure [3].

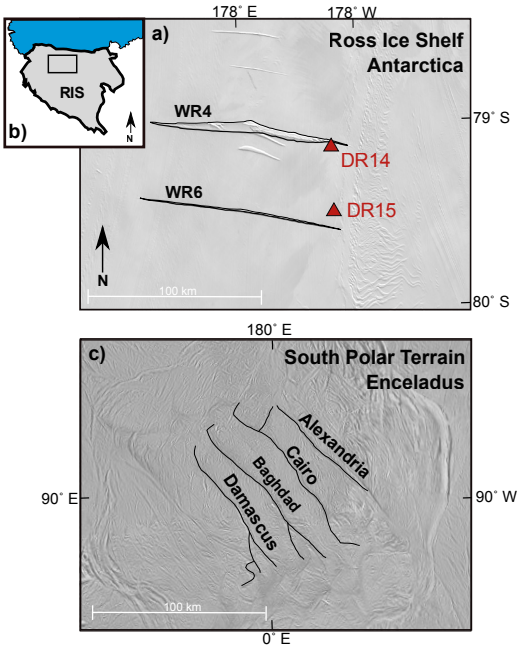

Figure 1. a) Map of study area on Ross Ice Shelf with (black outline) rifts WR4 and WR6, and (red triangles) seismometers DR14 and DR15. Background is MODIS 2014 satellite image. b) Geometry of (grey) full Ross Ice Shelf with black rectangle outlining area shown in a), (blue) ocean, and (white) grounded ice. c) Enceladus' South Polar Terrain with (black outline) the four Tiger Stripe fractures. Background is Enceladus Polar Map PIA14940, Cassini Imaging Team.

In advance of seismometer deployment on Enceladus or another ice-ocean world, a thorough understanding of the characteristics of ice-rift seismicity is needed. Floating ice shelves at the margins of Earth's polar ice sheets offer the closest terrestrial analog environment in which to investigate tidally driven ice-rift seismicity. We focus our study on two major fractures, or rifts, within the interior of the largest ice shelf in the world, the Ross Ice Shelf, Antarctica (Figure 1a). The rifts of interest are in the central portion of the Ross Ice Shelf and are in hydrostatic equilibrium with the ocean, presenting a similar environment to a planetary icy shell. The two rifts we study, WR4 and WR6 (Figure 1a), have similar lengths and widths to the Tiger Stripe Fractures, as well as similar inter-rift spacing. As the ocean tide traverses the sub-ice cavity during the daily tidal cycle, the two fractures experience across-rift tension (at falling tide) and compression (at rising tide).

We analyze two years of broadband seismic data recorded by two on-ice seismographs, one located adjacent to each rift (red triangles in Figure 1a). We detect 13,000 icequakes at rift WR4 and 4,000 icequakes at WR6 using an automated short-term average/long-term average detection algorithm, paired with manual event review. We attribute the difference in number of icequakes detected at the two rifts to the fact that seismic station DR15 was located four times as far from rift WR6 (~8 km) as seismic station DR14 was from rift WR4 (~2 km; Figure 1a).

Icequake Activity: Seismic activity at both ice-shelf rifts is strongly tidally modulated, with the highest levels of seismicity at each rift occurring at falling tide [4,5]. Specifically, the highest levels of seismic activity occur when both tensile stress across the rift and extension rate are high. At each rift we explore the distribution of icequake magnitudes to investigate the characteristics of tidally stressed, icy-fault seismicity and to characterize the dimensions of slip patches active in individual icequakes. Icequake magnitudes are small, ranging from moment-magnitudes, M_w, of -2 to 0.

We find that icequakes at each rift follow Gutenberg-Richter relationships, with slopes, known as b-values, close to 1.5 (Figure 2). This is higher than typical b-values (~1) observed in large populations of

tectonic earthquakes [6] and b-values of icequakes observed on other ice shelves [7]. We use the b-values we calculate to explore the scaling of stress drop at an ice-rift environment with respect to the slip distances and slip-patch areas active in individual seismic events. Well-constrained b-values for a tidally flexed, icy rift environment can be used to estimate the magnitude distribution of seismic events on a planetary body that lacks seismic observations, when combined with calculated values for the total release of seismic energy [8]. Our analog observational from the Ross Ice Shelf suggest that a b-value of ~1.5 is appropriate for Enceladus' Tiger Stripe Fractures.

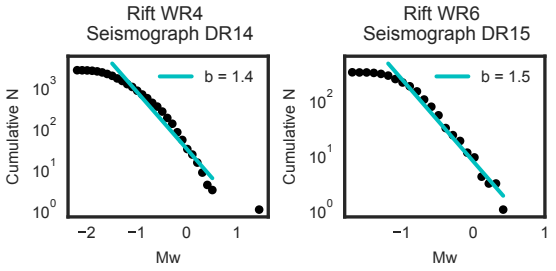

Figure 2. Gutenberg-Richter relationship for icequakes at each seismic station. Blue line shows calculated b-value at each station.

We explore the spectral characteristics of rift icequakes using Gaussian Mixture Models, an unsupervised-learning approach. At each rift we cluster events based on dominant frequency and a frequency-index parameter, calculated as the ratio of the amplitude-spectrum mean at two frequency bands [9]. We identify distinguishable populations of icequakes with higher (~30 Hz) and lower (~5 Hz) dominant frequencies (Figure 3a and b). This clustering analysis allows us to draw distinctions between multiple types of seismic activity recorded by a single on-ice seismic station and investigate the seismic source for each icequake type.

At each rift the majority of icequakes (>90%) fall within the lower-frequency group (blue events, Figure 3), and analysis of the polarization of icequake surface waves shows that these events originate from the direction of the closest rift (Figure 3c and d), providing strong evidence that these events are generated by rift deformation. A small number of icequakes recorded at each station (< 10%, red events, Figure 3) are dominated by higher-frequency energy and exhibit a range of back azimuths (Figure 3e and f). The higher-frequency content of these events suggests they may be generated by close to each seismic station, potentially through a mechanism such as contraction and small-scale surface fracture of the ice surrounding the seismograph [10]. We further explore details of the seismic sources by investigating physical and environmental conditions at

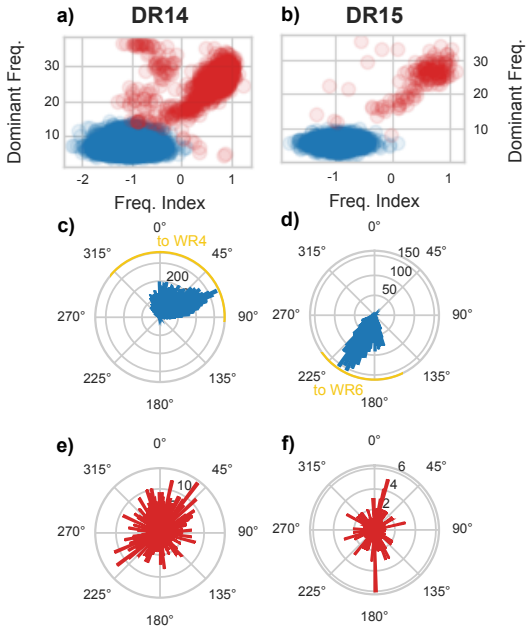

Figure 3. Icequakes recorded at station DR14 (left column) and DR15 (right column) clustered by frequency content. a and b) Red events have higher dominant frequencies, blue events have lower dominant frequencies. c and d) Polar histogram of back azimuths for lower-frequency icequakes at each station. Yellow arc identifies the direction of closest rift. e and f) Polar histogram of back azimuths for higher-frequency icequakes at each station.

the two rifts, such as the stress state, stretching rate across the rifts, and temperature at the time of individual icequakes.

This icy-ocean-world analog study demonstrates the valuable information that can be gained from a single seismic station deployed within several kilometers of a tidally flexed ice fracture. We explore what new findings from Ross Ice Shelf icequakes may mean for Enceladean seismicity, and how the analysis techniques described here could be employed to analyze seismic data collected by a future lander along the Tiger Stripe fractures. Findings from this investigation provide new insights into seismic-energy release within an icy-rift environment, and demonstrate the utility of terrestrial ice shelves as planetary analogs.

References: [1] Porco et al. (2006) *Science, 311,* 1393-1401. [2] Patthoff & Kattenhorn (2011) *Geophysical Research Letters, 38,* 1-6. [3] Vance et al. (2018) *Astrobiology, 18,* 37-53. [4] Olsen et al. (2021) *JGR: Planets, **in prep.*** [5] Olinger et al. (2019) *Geophysical Research Letters, 43,* 6644-6652. [6] Ekström, G. et al. (2012) *Phys. Earth Planet. Inter., 200,* 1-9. [7] Bassis et al. (2007) *J. of Glaciology, 53,* 523-536. [8] Hurford T. A. et al. (2020) *Icarus, 338,* 113466. [9] Buurman & West (2010) *USGS Professional Paper 1769,* Ch. 2. [10] Lombardi et al. (2019) *Annals of Glaciology, 60,* 45-56.